Maejo International Journal of
Energy and Environmental Communication

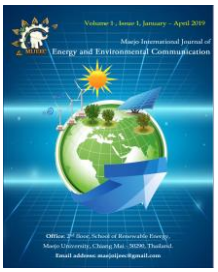

ARTICLE

Analysis on a vibration character of hollow fiber membrane bundle in MBR

Prattakorn Sittisom[1], Yoonjae I[2], Tomoaki Itayama[1]*

[1]Graduate School of Engineering, Nagasaki University, Nagasaki 852-8131, Japan.
[2]Membrane Department, Mitsubishi Chemical Co., Ltd., Japan

* Corresponding author, E-mail address: itayama@nagasaki-u.ac.jp

ARTICLE INFOR

Received 02nd November 2019
Accepted 20th December 2019

Keywords:
MBR
Membrane fouling
Membrane vibration
High-speed camera
Accelerometer

ABSTRACT

We have focused on membrane vibration in MBR to find an effective design for the reduction of membrane fouling. In the previous study, we developed a direct measurement method for membrane vibration of a hollow fiber membrane (HFM) using an accelerometer (ACM). In this study, we studied on vibration characters on an HFM bundle in a practical membrane module in MBR using the ACMs in a large transparent water tank. Three ACMs were attached at the middle (P1), top (P2) and bottom (P3) position along a center line in the HFM bundle in which air was supplied from a diffuser below the membrane module with different aeration rates from 0 to 250 L/min. The acceleration of membrane vibration time series for the X-axis direction (left-right displacement) and Z-axis direction (back-front displacement) was recorded at three positions. The average vibration amplitudes of the acceleration along both directions at each position were increased as the aeration rate was increased. The HFM bundle showed a collective vibration with a frequency peak between 0 and 50 Hz. The Z-axis motion character of HFM bundle is regarded as a sheet vibration. The obtained vibration character was useful for the new design of a membrane module in MBR against the membrane fouling.

1. Introduction

Membrane bioreactors (MBRs) using microfiltration membrane (MF) such as hollow fiber membrane (HFM) have been used widely in wastewater treatment as an application because MBRs can produce high water quality with minimized space and sludge production. In the development of MBRs, the technical improvement of MBRs has the for the countermeasure of the membrane fouling (Li et al., 2013). The goal has led to several techniques for continuously preventing the accumulation of scale and solids cake on the membrane surface which causes the membrane fouling to noticeably reduce the filtration capacity (Kirker, 2007). Hence, many researches have been performed to control and reduce membrane fouling.

The use of bubbling has been commonly adopted in MBRs for keeping the filtration capacity (Bellara et al., 1996). The concentration polarization layer of solid suspensions and membrane foulants around the membrane, which limits the filtration rate, can be suppressed by the flow on the membrane surface induced by the rising of bubbles (Cheng et al., 1998). Also, the rising bubbles directly correlated to the membrane vibration which affects for prevention of membrane fouling (Cabassud et al., 1997). It was thought that the surface turbulent flow by bubbles and the direct collision of bubbles to the membrane cause the membrane vibration (Cui et al.,

2003). It was succeeded in measuring the fluctuating shear stress by the stress sensor and the fluctuation motion of the flat sheet membrane by the laser displacement sensor (Sakai et al., 2014). The vibration of hollow fiber membranes in a model MBR chamber made of transparent plastic was measured by using a high-speed camera (HSC) (Sittisom et al., 2020). Then the analysis results were effectively applied to improve the design of the membrane module (Sittisom et al., 2020). Thus, the monitoring of the membrane vibration in an MBR is very useful for the design of a membrane module or unit to suppress the membrane fouling effectively.

However, it is complicated to measure the membrane vibration in a practical MBR using such optical methods such as HSC because of the high turbidity of sludge suspension in an MBR chamber. For the purpose, we developed the measurement method using an accelerometer (ACM) (Sittisom et al., 2020). It was succeeded to measure membrane vibration using the ACM attached to an HFM (Sittisom et al., 2020). In the experiment to clarify the effect on the vibration of a single string HFM with the different looseness, the comparison between ACM measurement and HSC measurement was performed. Then we used the turbulence flow generated by the submerged pump to causer the membrane vibration. It presented the complete identical results for both measurement methods that the root mean square of the acceleration of the membrane vibration decreased as the looseness increased (Sittisom et al., 2020).

In the experiment, a sensor was set on a single string membrane. However, practical MBRs use several membrane modules in which many HFM strings were bundled with high density. It is thought that the motion of the HFM can show the character of the collective motion of the HFM bundle. Therefore, the character of the vibration may be considerably different from the vibration of a single string of HFM.

In this study, to fill the knowledge gap on the vibration character of HFM bundles, we conducted the experiment using a practical scale membrane module in a test chamber. The vibration was measured using ACMs attached on the different positions on a string of a membrane to analyze the vibration character in each position in the membrane module, then the effect of the bubbling strength (air sparge rate) for the vibration character was measured because there has been no research to clarify these characters though the basic vibration characters must be essential to design the new membrane module and MBR system.

2. Experimental setup and methods

2.1 Experimental set-up

The experimental set-up for measuring the vibration of the membrane module is illustrated in Figure 1. A membrane module, which was consisted with PVDF hollow fiber membrane (Mitsubishi Chemical Co. Ltd., JAPAN) with the nominal pore diameter of 0.4 μm and the outer fiber diameter 2.8 mm, was set in water chamber (200cm width x 200cm length x 300cm height) as shown in Figure 1. The membrane fibers of 600 were embedded in the plastic moldings at the bottom and the top in the module (2.5cm width x 50cm length x 100cm height). The density of the hollow fiber membrane in the module was 12/cm^2. As hollow fiber membranes of 102 cm in length were set in the module, the looseness of the fiber was defined as 2% looseness. The air was sparged from the holes of 10 cm regular intervals on a PVC tube of 13cm in diameter. The airflow rate was changed as 60, 100, 160, 200 and 250 L/min in the experiment.

Nomenclature and Abbreviation

AC	Alternating current
ACM	Accelerometer
DFT	Discrete Fourier transformation
HFM	Hollow fiber membane
HSC	High-speed camera
MBR	Membrane bioreactor
MF	Microfiltration membrane
PDF	Probability density profile
PVDF	Polyvinylidene difluoride
RMS	Root mean square
SD	Standard deviation

Accelerometer (ACM) KXP84 (Kinonix, Inc., USA) of 0.049 g in weight, the size of 5mm x 5mm x 1.2mm (thickness) can measure the acceleration values for the three directions (X, Y, Z), as shown in Figure 1(c). Before the experiment for HFM vibration measurement, the response of the ACM was tested in different frequencies from 0 to 500 Hz by vertical and horizontal vibration testing machine (LABTONE, Labtone Test Equipment, Co., Ltd.) at Nagasaki Industrial Technology Center. The detail was described in our previous report (Sittisom et al., 2020).

The X, Y and Z directions of the ACM for the sensing were defined in Figure 2(b). The three ACMs were attached on a string of HFM surface at 10cm (top), 50cm (middle) and 90cm (bottom) below from the top end of the HFM with UV resin of 0.1 g to measure the acceleration values at the three positions. X-direction of each ACM was set along the left and right direction of the HFM module shown in Figure 2(b). Z-direction of each ACM was along the front and back direction. Y-direction of each ACM was along the up and down direction. The values of acceleration data of X and Z as analog voltage (660 mV/G) were transmitted to a data logger of 12bit ADC (DS1M12, Company name) using polyurethane coated thin copper wires (0.06 mm diameter, 450 mm length). Six wires for one sensor were totally connected to the ACM including three data lines, a positive power supply (6 V), ground and the logic line for data acquisition enable. The

6 wires were passed through inside the hollow fiber membrane. The total weight of the 6 wires was 0.08 g. Thus, the total weight of the assembled ACM was 0.229 g for one sensor. Thus, three sensors of total 0.687g were attached to the HFM of 2.03 g weight. The analog data lines from the accelerometer were connected to the ground through a capacitance of 0.033μF, according to the company's instruction manual for the high-frequency noise reduction. The time interval for data collection of the data logger was set with 1.00 msec period for 60 seconds. The measurement was

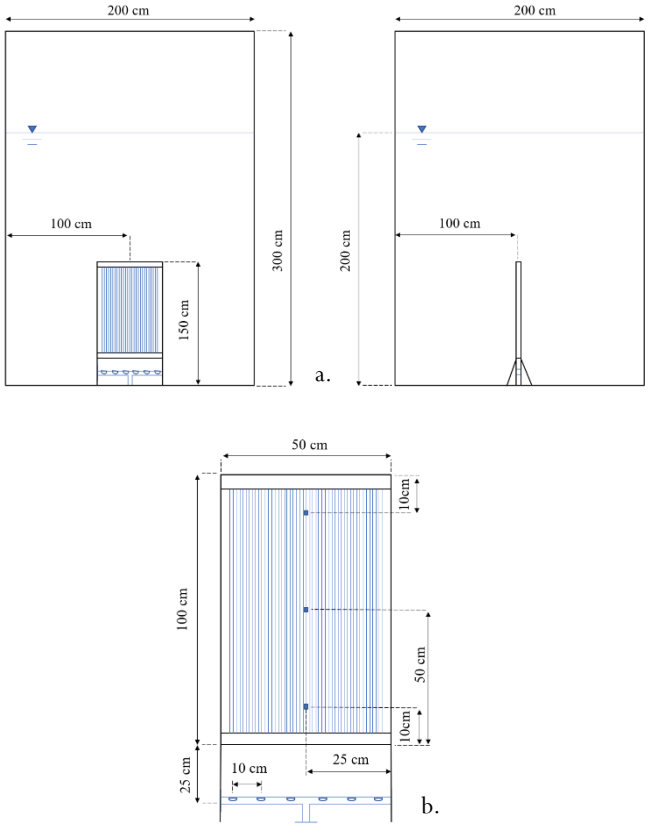

Figure 1. Experiment Set-up a. Side-Front view of MBR b. Aluminium case with ACM-attached membrane module

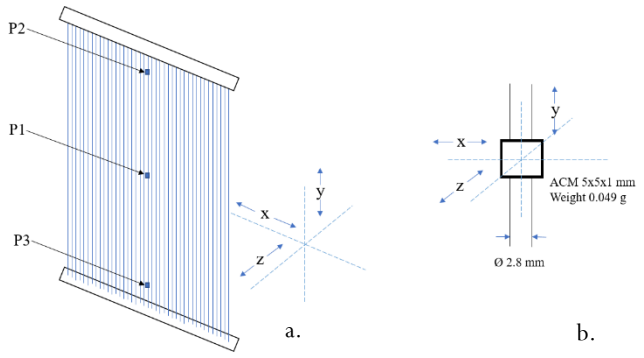

Figure 2. Reference axis a. Module reference axis b. ACM reference axis

2.2 Data Processing

The average was subtracted from each acceleration time series data (mean centering). Then Butterworth band stop filter (6th order) was applied to remove electric noise 60Hz and its harmonic frequency in software package "dplR". The width of the stop frequency region was designed as 4 Hz.

The probability density function (PDF) of acceleration was estimated for all data points of three repeating measurement data using the function "density" in the software R. Root mean square (RMS) value of acceleration time series $a(k)$ as an indicator of the strength of the random vibration corresponds to the standard deviation (SD) of the estimated probability density function as shown in the following equation (1).

$$RMS = SD = \sqrt{\frac{1}{N}\sum_{k=0}^{N-1}(a(k) - < a(k) >)^2} \quad \ldots (1)$$

Where $< a(k) >$ is the mean value.

In order to analyze the acceleration data with finite measurement time T in frequency domain, Discrete Fourier transformation (DFT) defined by equation (2) was applied for each time series (Brigham, 1988). The DFT was calculated by "fft" command with the hamming window in the package "Signal (ver.0.6-7)" in the R. Then the power spectrum density was calculated by use of the following equation (3) (Brigham, 1988).

$$P(f) = |Fa(f:T)|^2 / T \ldots (3)$$

Then the power spectrum densities for three repeating measurements were averaged to one power spectrum density. The averaged power spectrum density was smoothed by using "ksmooth" function in the R to present distinct peaks in the spectrum. Furthermore, in order to test the numerical error of the FFT calculation and the power spectrum density calculation, Parseval's identity was tested between the frequency domain data and the original time-domain data (Brigham, 1988). Both calculation results for sinusoidal time-series test data matched in all seven digits.

3. Results and Discussion

3.1 Measurement of membrane vibration using ACM

The periodic noise in the measurement data by the three ACMs was observed under the still water condition without aeration as shown in Figure 3. After converting the data to the power spectrum density, a peak at 60 Hz and every harmonic frequency of its had been detected. It was clear that the noise was originated from the electric power line because AC electric power of 60Hz is used in the area where we conducted the experiment (Toyohashi city, Aichi, Japan). Therefore, the peak of 60Hz and the four major harmonic peaks (120Hz, 180Hz, 320Hz, 480Hz) were removed by use of the stop band filter for each frequency as mentioned in Materials and Methods.

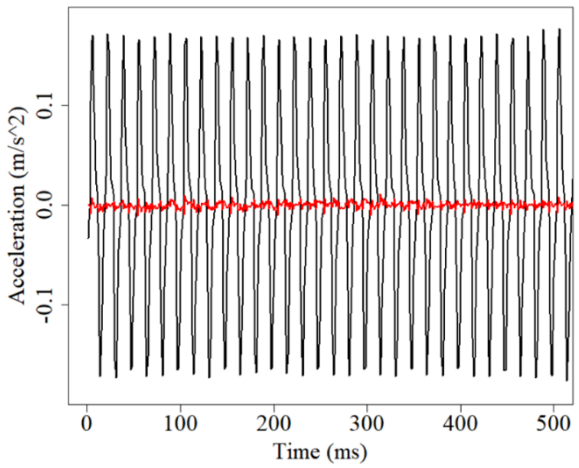

Figure 3. Acceleration time series measured by ACM under the condition without aeration

Figure 4 (Figure 5) shows PDFs of the acceleration of the motion of HFM bundle for X (Z) direction with different aeration rates. The shape of each PDF is similar to a gaussian function (normal distribution) of the center peak (mean) at zero through the width of each PDF was different. According to Figure 2(b), X and Z direction are perpendicular for gravity direction (Y direction) in the conFiguration of each ACM. However, it is impossible to exactly set the sensor with this conFiguration. Thus, a small component of gravity acceleration could remain as a small bias. However, the time average of acceleration of a vibration motion should be zero. Otherwise, a vibrating object causes an acceleration motion for a direction, then it must go out to the water chamber. Therefore, the mean centering of the acceleration time series can be justified. Then the shape of PDF, as already mentioned, is similar to gaussian function. It means that the time series of the acceleration could be recognized as a random process driven by random forces as gaussian noise. Because the aeration caused the turbulence of two-phase flow in our experiment setup, the motion of the HFM bundle was induced by the shear stress of the turbulence and the continuous collision of bubbles to membranes. These must give random forces to each membrane string; then it is apparent that the stronger aeration provides a stronger random force. Figure 4 and Figure 5 presents the increase of the width of each PDF as the aeration increased. Because SD (RMS) of the acceleration means the average strength of vibration motion, it resulted that the higher aeration caused the higher acceleration motion of the HFM as shown in Figure 6 and Figure 7. The vibration strength as SD value in the acceleration along the X-axis direction at the bottom (P3) was largest, the second strong vibration was detected at the middle position (P1), and the weakest vibration was at the top position (P2). It is a reasonable result because the bubble density was highest at the bottom near the air diffuser place. In addition, the kinetic energy of the fluid motion was dispersed along the upward direction (Y-axis direction) because the average flow of two-phase turbulence was up-flow.

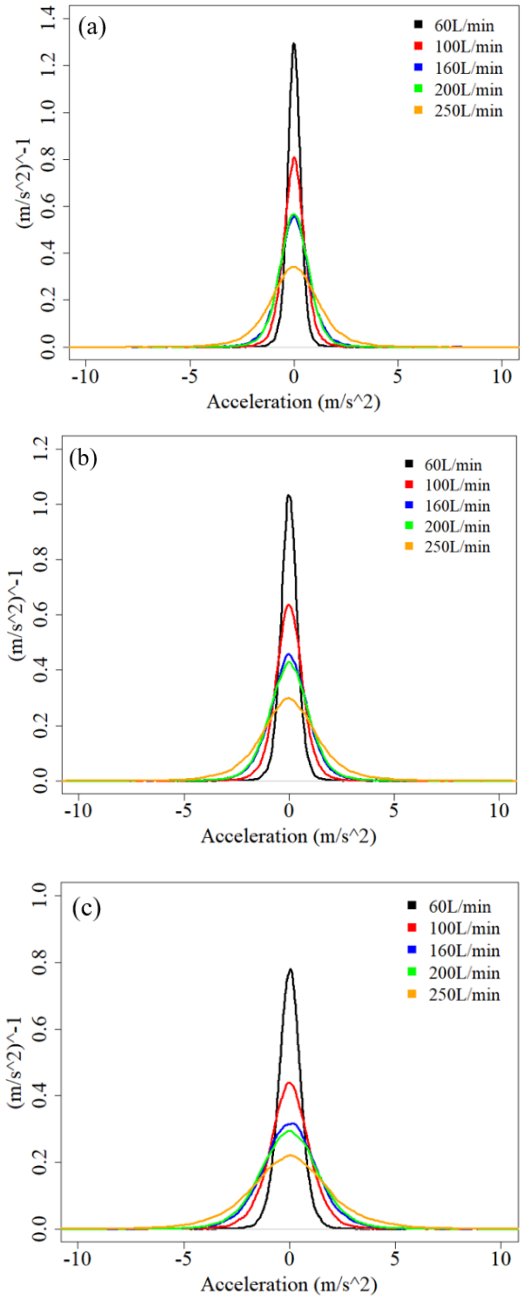

Figure 4. Probability density of the measured values of the acceleration at Middle position (X-axis)
The data was obtained by the ACM for each aeration rate (60, 100, 160, 200 and 250 L/min)
a. Top position (P2) b. Middle position (P1) c. Bottom position (P3)

It means that the shear force on the membrane surface at the bottom was largest, the second was middle, the smallest was the top. The results in Figure 6 showed the same as this order.

However, the response character for the change of airflow rate at the middle position and the order of strength of vibration for the position were not trivial in the Z-axis direction. There was no significant increase of SD value of the acceleration along the Z-axis direction despite the clear increase along X-axis direction at the middle point was observed.

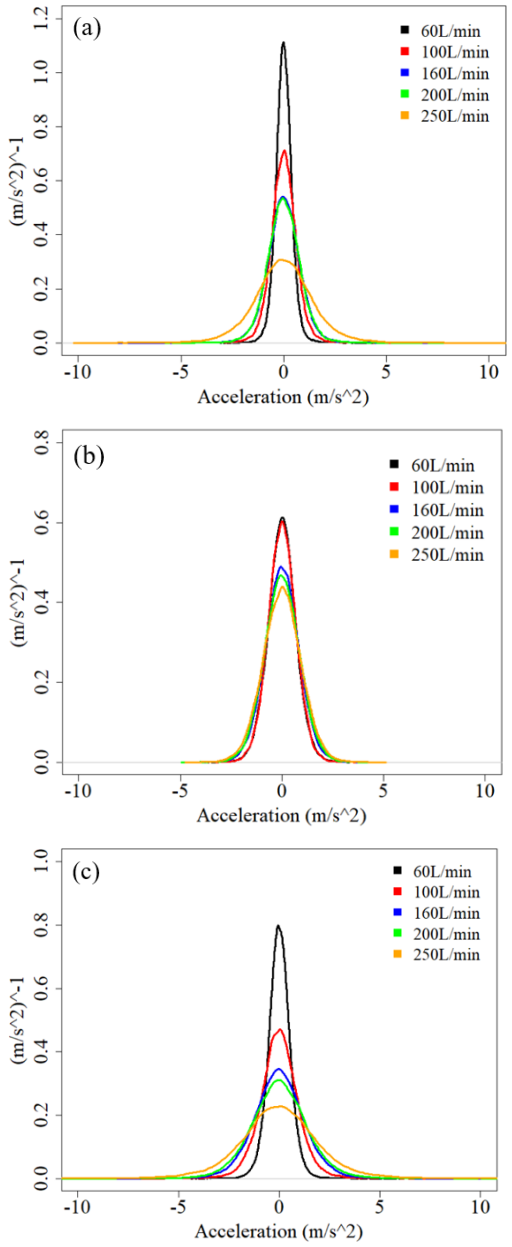

Figure 5. Probability density of the measured values of the acceleration at Middle position (Z-axis).
The data was obtained by the ACM for each aeration rate (60, 100, 160, 200 and 250 L/min)
a. Top position (P2) b. Middle position (P1) c. Bottom position (P3)

Especially, the strongest vibration (SD) of Z-axis direction was observed in the middle position at the lowest airflow rate of 60 L/min. But, in higher airflow rate conditions, the vibration strength (SD) for Z-axis direction at the middle position was lower than the other positions as shown in Figure 7.

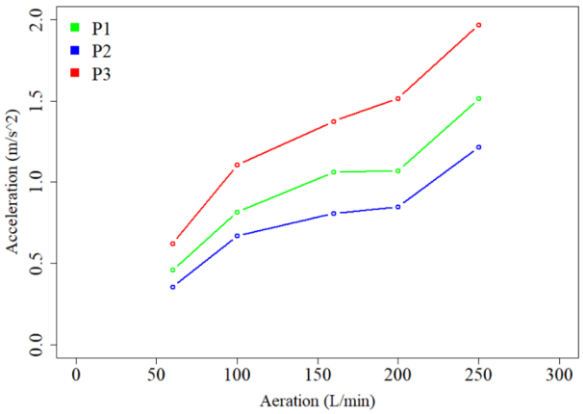

Figure 6. Standard Deviation of acceleration from ACM (X-axis)

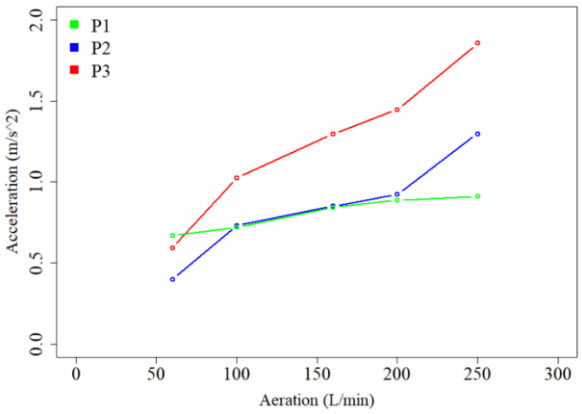

Figure 7. Standard Deviation of acceleration from ACM (Z-axis)

Considering the structure of the HFM bundle and the diffuser, such anisotropic response could be involved by the water flow by the rising bubbles from the diffuser. Namely, the membrane buddle in the module was laid between the upward flows at both sides of the membrane bundle by the collective rising bubbles (see Figure 1). It was thought that the upward flow velocity by the bubbles was higher near the HFM bundle. Then the flow velocity might decrease as it was further from the HFM bundle. According to the Bernoulli theorem in fluid dynamics, the pressure at higher velocity is lower than the pressure at a lower velocity (Landau et al., 1987). Therefore, the pressure gradient filed could cause the velocity component of Z-axis direction to the HFM from both sides. The water flow toward the HFM bundle on both sides will push the membrane from both sides and may limit the movement of the membrane in the Z-axis direction. It was found that the acceleration for the Z-axis direction was slightly lower than that for X-axis direction. Moreover, the HFM bundle might show a motion similar to a two-dimension membrane sheet due to both sides press from both sides. In addition, although the boundary conditions at the top and bottom were fixed boundary, the boundary conditions at the

left and right sides were a moving free boundary if the membrane sheet vibration is assumed. Therefore, the first mode of the sheet (membrane bundle) vibration as a standing wave in the Z-axis direction along the X-axis was the inverse phase vibration at the left side and the right side. The P1 position was a loop of the standing wave for the first mode along the Y-axis. However, considering the standing wave for X-axis, the second mode of the standing wave for the Y-axis was easier excited because the P1 position at the centerline between the top and the bottom was a fixed point. Under the interpretation of a vibrating rectangular sheet for the Z-axis direction, the sensor of P1 at the center was a special position at which the two-node lines along the X-axis and Y-axis of sheet vibration were crossed. Namely, a two-dimensional standing wave (vibration) was excited as shown in Figure 8.

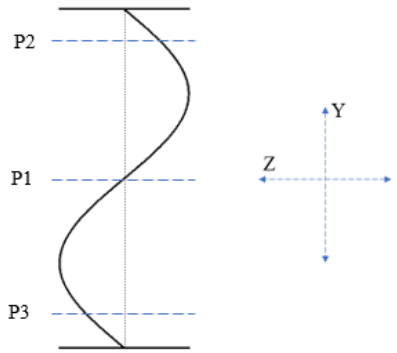

Figure 8. Standing wave vibration with reference axis (Side view)

Obviously, the observed acceleration has consisted with the summation of many kinds of vibration components with different frequencies. The collective motion of the membrane buddle, which can be regarded as a sheet vibration, may have a lower frequency than the other vibration of a single string due to the difference of the total mass.

To analyse the detail of the vibration character, power spectral densities (power spectrum) of the acceleration of the HFM vibration were computed. The power spectrums for the X-axis direction at the 3 positions under the different aeration rate are shown in Figure 9 and those for the Z-axis direction were shown in Figure 10. The dips at 60Hz and the harmonic frequencies are found in each spectrum because of the stopband filter to cut the electric noise from AC power line with 60 Hz. Each dip is enough sharp and narrow in the frequency bandwidth. Therefore, it was considered that the effect of the filtering was not significant.

The power spectrum for the Z-axis direction at P1 is very different from the other spectrum as shown in Figure 10 (b) because the position of P1 at the center of the HFM bundle is a node position of a sheet vibration for X-axis and Y-axis as already discussed. Notably, the vibration lower than 50Hz was apparently weaker at P1 position comparing to the vibration strength of this frequency region at P2 and P3. Therefore, the vibration of a lower frequency than 50Hz could correspond to a collective vibration for the Z-axis direction of the HFM bundle. On the other hand, the power spectrum at P1 in the frequency region between around 150Hz to 200Hz increased by the increment of aeration rate.

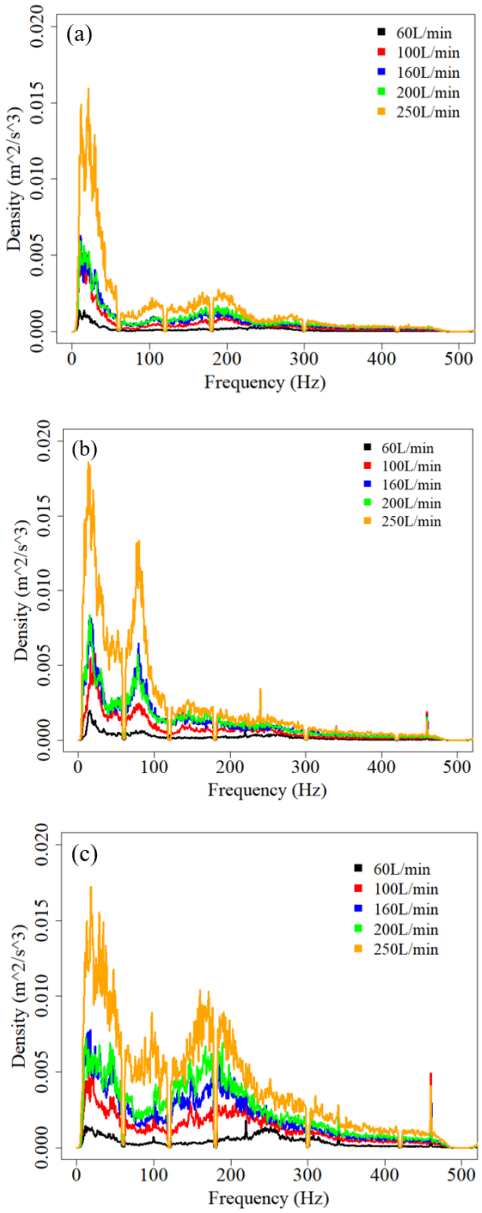

Figure 9. Power spectrum density of acceleration from ACM (X-axis)
a.Top position (P2) b. Middle position (P1) c. Bottom position (P3)

Then, as the aeration increased, the power spectrum of the vibration for the Z-axis direction at the P1 and P3, and that for X-axis at P3-axis direction increased in this frequency region as shown in Figure 9 and Figure 10 (c). It means that the direct effect for each.

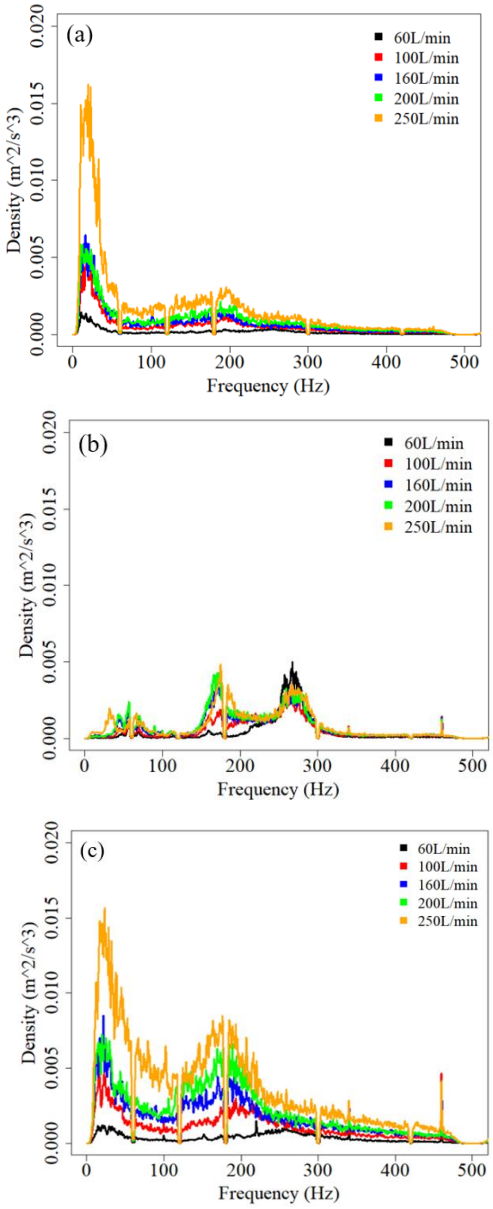

Figure 10. Power spectrum density of acceleration from ACM (Z-axis)
a.Top position (P2) b. Middle position (P1) c. Bottom position (P3)

HFM by the bubble collision and the share force of turbulence could excite the vibration in this frequency region because both peaks of the X-axis direction and Z-axis direction were higher at P3 position near the air diffuser than the other position. However, the peaks between 250Hz and 300Hz in power spectrums for Z-axis direction at P2 (middle position) were not affected by the difference of the aeration strength.

It is not so clear to give an interpretation on the phenomena. It is necessary to conduct a further investigation of the turbulence of two-phase flow near the HFM bundle to understand the vibration phenomena of the HFM bundle. Such fundamental studies must provide a new idea for the structure of the HFM module to mitigate the membrane fouling.

4. Conclusion

This study measured directly on membrane vibration from 2-phase flow for the membrane bundle. We observed membrane vibration from ACM in different positions, Middle (P1), Top (P2) and Bottom (P3). This study concluded the following: (1) Bottom (P3) position of HFM can be induced sharply from diffuser; and (2) - HFM vibration showed strong acceleration for x-axis.

Acknowledgments

The authors gratefully acknowledge Mr.Yoonjae I and all staff at Membrane Department of Mitsubishi Chemical Co Ltd. who provided an opportunity to conduct the experiment and gave access to the laboratory and research facilities.

References

Bellara S.R., Cui Z.F., Pepper D.S., 1996. Gas sparging to enhance permeate flux in ultrafiltration using hollow fiber membranes. Journal of Membrane Science 121(2): 175.

Brigham E.O., 1988. The Fast Fourier Transform and Its Application. Englewood Cliffs, New Jersey.

Cabassud C., Laborie S., Laine J.M., 1997. How slug flow can improve ultrafiltration flux in organic hollow fibres. Journal of Membrane Science 128(1): 93.

Cheng T.W., Yeh H.M., Gau C.T., 1998. Enhancement of permeate flux by gas slugs for crossflow ultrafiltration in tubular membrane module. Journal of Membrane Science 33 (15): 2295.

Cui Z.F., Wright K.I.T., 1994. Gas–liquid 2-phase crossflow ultrafiltration of BSA and dextran solutions. Journal of Membrane Science 90(1/2): 183.

Cui Z.F., Wright K.I.T., 1996. Flux enhancements with gas sparging in downwards crossflow ultrafiltration: performance and mechanism. Journal of Membrane Science 117(1/2): p. 109.

Cui Z.F., Chang S., Fane A.G., 2003. The use of gas bubbling to enhance membrane processes. Journal of Membrane Science 221(1/2): p. 1.

Kirker C., 2007. Cleaning hollow core membrane fibers using vibration. United States Patent, US 7,282,147 B2.

Landau L.D., Lifshitz E.M., 1987. Fluid Mechanics. 2nd Edition., Elsevier Science, Netherlands.

Li T., Law A.W.K., Cetin M. and Fane A.G., 2013. Fouling control of submerged hollow fibre membranes by vibrations. Journal of Membrane Science 427, 230-239.

Ozaki N., Yamamoto K., 2001. Hydraulic effects on sludge accumulation on membrane surface in cross flow filtration. Water Research 35(13): p. 3137.

Richard W.H., 1997. Digital Filter. 3rd Edition., Dover Publications, New York.

Sakai S., Nagaoka H., Inoue M., 2014. Measurement of vibration patterns of flat-sheet membrane module induced by aeration using laser displacement meters in MBRs, Journal of Environmental Engineering Research 70(7): pp. III 165-173

Sittisom P., Itayama T., 2020, Analysis on a vibration character of hollow fiber membrane for MBR using a high-speed camera and an accelerometer. Journal of Faculty of Engineering, Chiang Mai University Vol.27(1).

Taha T., Cui Z.F., 2002. CFD modelling of gas-sparged ultrafiltration in tubular membranes. Journal of Membrane Science 210(1): p. 13.

Xia L., Law A. W. K., Fane A. G., 2013. Hydrodynamic effects of air sparging on hollow fiber membranes in a bubble column reactor. Water Research 47: 3762-3772.